

Supporting Information

**Water-soluble room temperature long afterglow carbon dots/silica
composites for dual-channel detection of alkaline phosphatase and
multi-level information anti-counterfeiting**

*Xiangying Sun**, *Wei He*, *Bin Liu*

*College of Materials Science and Engineering, Huaqiao University, Key Laboratory
of Molecular Designing and Green Conversions (Fujian University), NO. 668 Jimei
Avenue, Jimei District, Xiamen 361021, China*

To whom correspondence should be addressed:

**(Xiangying Sun) E-mail: sunxy@hqu.edu.cn*

1. Experimental section

1.1 Materials and instruments

Materials. Phosphoric acid, sulfuric acid, ammonia, ethylene glycol, ethylenediamine, ethanolamine, urea, starch, sodium chloride, polyethylene glycol, boric acid, magnesium sulfate and p-nitrophenol were purchased from Sinopharm Chemical Reagent Co., Ltd (Shanghai, China). Tetraethoxysilane, 3-aminopropanol, diethanolamine, triethanolamine, o-aminophenol, m-aminophenol and p-aminophenol were purchased from Aladdin (Shanghai, China). Sodium p-nitrophenyl phosphate was supplied by Macklin(Shanghai, China). Alkaline phosphatase was purchased from Sangon Biotech Co., Ltd. (Shanghai, China). Ultrapure water was prepared by a Milli-Q water purification system (USA).

Instruments. All fluorescence spectra were recorded by a HITACHI F-7000 fluorescence spectrometer (Hitachi, Japan). Absorption spectra were measured with a UV-2600 UV-Vis spectrophotometer (Shimadzu, Japan) and a Cary 5000 UV-Vis-NIR spectrophotometer (Agilent, USA). Morphology of samples was recorded by transmission electron microscope (TEM, FEI Talos F200s, America). Fluorescence and afterglow lifetime decay curves were obtained by employing a FS5 fluorescence spectrometer (Edinburgh Instruments, UK). Fluorescence quantum yield and afterglow quantum yield were measured with a FLS920 fluorescence spectrometer (Edinburgh Instruments, UK) and a FLS980 fluorescence spectrometer (Edinburgh Instruments, UK), respectively. X-ray diffraction (XRD) was performed using a Rigaku SmartLab. The X-ray photoelectron spectra (XPS) were recorded on a

Quantum-2000 electron spectrometer (Physical electronics Co., Ltd). The Fourier transform infrared (FTIR) spectra were taken by a FTIR-4800s spectrophotometer (Shimadzu Co., Ltd). Zeta potential and dynamic light scattering size distribution were obtained by a Zetasizer Nano ZS (Brookhaven Instruments Corporation, America).

1.2 Synthesis of other types of CDs

1.0 mL of 3-aminopropanol (diethanolamine, triethanolamine, o-aminophenol, m-aminophenol, p-aminophenol, ethylenediamine, or ethylene glycol) was added to 15 mL of deionized water. 2 mL of phosphoric acid was added dropwise accompanied by vigorous stirring to form a uniform and transparent solution. Next, the above solution was transferred to a household microwave oven to react for 150 seconds. Once the initial product cooled down to room temperature, 20 mL of water was added for dispersion. Subsequently, the mixed solution was centrifuged at high speed to remove large particles, and then the supernatant was filtered through a 0.22 μm membrane to obtain CDs-1, CDs-2, CDs-3, CDs-4, CDs-5, CDs-6, CDs-7, CDs-8 are obtained, respectively.

1.0 mL of ethanolamine was added to 15 mL of deionized water. 2 mL of sulfuric acid was added dropwise accompanied by vigorous stirring to form a uniform and transparent solution. Next, the above solution was transferred to a household microwave oven to react for 150 seconds. Once the initial product cooled down to room temperature, 20 mL of water was added for dispersion. Subsequently, the mixed solution was centrifuged at high speed to remove large particles, and then the

supernatant was filtered through a 0.22 μm membrane to obtain CDs-9.

1.0 mL of ethanolamine was added to 15 mL of deionized water. 2 mL of phosphoric acid was added dropwise accompanied by vigorous stirring to form a uniform and transparent solution. Next, the above solution was hydrothermally reacted at 200 $^{\circ}\text{C}$ for 6 h or pyrolyzed at 200 $^{\circ}\text{C}$ for 1 h. The samples were cooled to room temperature to obtain CDs-10 and CDs-11.

1.3 Synthesis of other types of CDs/SiO₂ composites

0.5 mL of CDs solution (CDs-1, CDs-2, CDs-3, CDs-4, CDs-5, CDs-6, CDs-7, CDs-8, CDs-9, CDs-10 and CDs-11) and 2.5 mL of tetraethyl orthosilicate (TEOs) were added to 25 mL of deionized water and stirred for 5 minutes to form a homogeneous solution. Next, 0.5 mL of ammonia aqueous ($\text{NH}_3\cdot\text{H}_2\text{O}$) solution was added to the solution. After stirring at a temperature of 60 $^{\circ}\text{C}$ for 7 hours, the resulting product was dialyzed in a dialysis bag (3500 Da) against deionized water for a week. Later, the product was filtered three times through a 0.22 μm membrane, and the CDs/SiO₂ aqueous solution (CDs-1/SiO₂, CDs-2/SiO₂, CDs-3/SiO₂, CDs-4/SiO₂, CDs-5/SiO₂, CDs-6/SiO₂, CDs-7/SiO₂, CDs-8/SiO₂, CDs-9/SiO₂, CDs-10/SiO₂ and CDs-11/SiO₂) was obtained.

2.5 mL of tetraethyl orthosilicate (TEOs) were added to 25 mL of deionized water and stirred for 5 minutes to form a homogeneous solution. Next, 0.5 mL of ammonia aqueous ($\text{NH}_3\cdot\text{H}_2\text{O}$) solution was added to the solution. After stirring at a temperature of 60 $^{\circ}\text{C}$ for 7 hours. Then 0.5 mL of CDs solution was added to the above solution and stirred at 60 $^{\circ}\text{C}$ for 7 hours. The resulting product was dialyzed in a dialysis bag

(3500 Da) against deionized water for a week. Later, the product was filtered three times through a 0.22 μm membrane, and the CDs/SiO₂-a aqueous solution was obtained. Lastly, CDs/SiO₂-a powder was obtained by freeze-drying the solution for 72 hours.

1.4 Synthesis of CDs-I and CDs-I/starch composites

CDs-I were synthesized by one-step hydrothermal method. 100 mg safranin T (ST) was added in 20 mL 0.5 M NaOH solution, and the solution was sonicated for 10 min to completely dissolve ST. Then, the mixed solution was transferred into a 50 mL polytetrafluoroethylene lined autoclaves and heated at 200 °C for 5 h. After the solution was naturally cooled to room temperature, it was stored in a refrigerator at 4 °C.

2 mL of CDs-I aqueous solution and 2 g of starch were dispersed in 40 mL of deionized water to form aqueous solution. After stirring the mixed solution for 12 h at room temperature, centrifuge for 10 minutes, remove the supernatant, and place the solid in a 60 °C oven to dry for 24 h to obtain CDs-I/starch powder.

1.5 Synthesis of different CDs-based composites

CDs/Biuret. 0.5 mL of CDs aqueous solution were mixed with urea (6 g) to obtain CDs-I/urea solutions in beakers by shaking for 10 min to completely dissolve the urea. Then the beakers were put into oven at 155 °C for 6 h. Urea will be converted to biuret. Cooled down to room temperature naturally. The final products (CDs/Biuret) were ground into powder.

CDs/NaCl. 0.5 mL of CDs aqueous solution were added to saturate NaCl solution

and stirred for 10 min. Then the mixed solution was added to the bottom of methanol solution, after standing for 48 h, CDs/NaCl was precipitated, and the product was ground into powder.

CDs/PVA. 0.5 mL of CDs aqueous solution were firstly diluted with 0.3 mL of deionized water. Then mixed with 1.5 mL of polyvinyl alcohol (PVA) solution (1.0 g in 15 mL water). Then dry the sample in a 60 °C oven for 6 h to obtain CDs/PVA film.

CDs/starch. 0.5 mL of CDs aqueous solution and 2 g starch were dispersed in 40 mL of deionized water to form aqueous solution. After stirring the mixed solution for 12 h at room temperature, centrifuge for 10 minutes, remove the supernatant, and place the solid in a 60 °C oven to dry for 24 h to obtain CDs/starch powder.

CDs/B₂O₃. 2 g of boric acid was dissolved with 40 mL of deionized water, and the solution was mixed with 0.5 mL of CDs aqueous solution in a beaker by ultrasonic for 10 min. Then the beaker was covered with foil to prevent the water from evaporating too fast. Afterwards, the beaker was put in an oven at 180 °C for 5 h. After the solution was naturally cooled down to room temperature, the amorphous glassy state composites were obtained. The final products (CDs/B₂O₃) were ground into powder.

1.6 Measurement of luminous lifetime

Multi-exponential function is used to fit the fluorescence and afterglow decay curves. The fitting equation is as follows[1]:

$$Y(t) = \sum_i A_i e^{-\frac{t}{\tau_i}} \quad (S1)$$

where A_i and τ_i respectively represent the weight of each process of the multi-exponential decay curve and the fluorescence or afterglow lifetime

1.7 Measurement of quantum yield

Fluorescence quantum yield: The fluorescence quantum yield was calculated according to the following equation[2]:

$$\varphi_S = \varphi_R \frac{Grad_S \eta_S^2}{Grad_R \eta_R^2} \quad (S2)$$

where S and R refer to standard group and test group (CDs solution), respectively; φ represents fluorescence quantum yield. A is the absorbance, G_{rad} means the gradient from the plot of integrated fluorescence intensity against absorbance; and η is the refractive index of the solvent (1.33 for water). Fluorescence quantum yield (φ_R) of quinine sulfate (0.1 M H₂SO₄) is 0.54 under 360 nm excitation.

Afterglow quantum yield: The afterglow quantum yield of the samples was measured by a FLS980 spectrometer with a calibrated integrating sphere in. In principle, the afterglow quantum yield can be expressed by the following[3]:

$$\varphi = \frac{\varepsilon}{\alpha} = \frac{\int_{360}^{700} L_{emission}}{\int E_{reference} - \int E_{sample}} = \frac{\text{number of emitted photons}}{\text{number of absorbed photons}} \quad (S3)$$

where φ is the afterglow quantum yield, ε is the emitted photons of the sample that were collected by the integrating sphere in the range of 360-700 nm, and α is the photons absorbed by the sample. $L_{emission}$ is the net luminescence of the sample.

$E_{\text{reference}}$ is the absorption spectrum of the reference in the sphere. E_{sample} is the absorption spectrum of the sample and reference.

1.8 The effects of different matrixes on the long afterglow effect of carbon dots

In addition, the effects of different matrixes on the long afterglow performance of CDs were studied. As illustrated in Figure S3a, starch, boron oxide, biuret and SiO₂ can effectively activate RTP of CDs in the solid phase. In addition, SiO₂ can also activate RTP of CDs in the liquid phase, but biuret, boron oxide, and starch as matrixes can't activate RTP of CDs in the liquid phase (Figure S3b). This is because boron oxide and biuret in water will be hydrolyzed into boric acid and urea, resulting in the loss of the protection of CDs. Starch in water cannot protect CDs, so RTP in the solution phase cannot be activated. SiO₂ can still exist in the form of SiO₂ network in aqueous solution and forms a strong C-O-Si covalent bond with CDs. The gel formation process of SiO₂ usually includes hydrolysis and condensation reactions. As shown in Figure S4, in reaction 1, TEOs can be hydrolyzed to form intermediate product 1, and then according to reaction 2, the hydroxyl groups on the surface of CDs can react with TEOs. Finally, the CDs were encapsulated in SiO₂ to form CDs/SiO₂ composites.

2. Figure

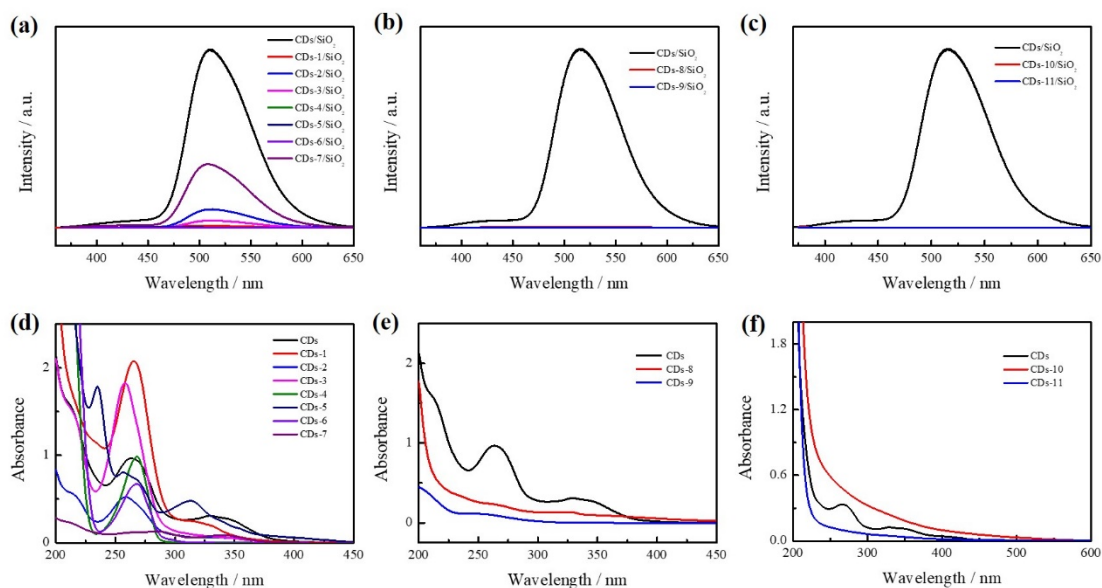


Figure S1. (a) Afterglow spectra of CDs/SiO₂, CDs-1/SiO₂, CDs-2/SiO₂, CDs-3/SiO₂, CDs-4/SiO₂, CDs-5/SiO₂, CDs-6/SiO₂ and CDs-7/SiO₂ composites. (b) Afterglow spectra of CDs/SiO₂, CDs-8/SiO₂ and CDs-9/SiO₂ composites. (c) Afterglow spectra of CDs/SiO₂, CDs-10/SiO₂ and CDs-11/SiO₂ composites. (d) UV-vis absorption spectra of CDs, CDs-1, CDs-2, CDs-3, CDs-4, CDs-5, CDs-6 and CDs-7. (e) UV-vis absorption spectra of CDs, CDs-8 and CDs-9. (f) UV-vis absorption spectra of CDs, CDs-10 and CDs-11.

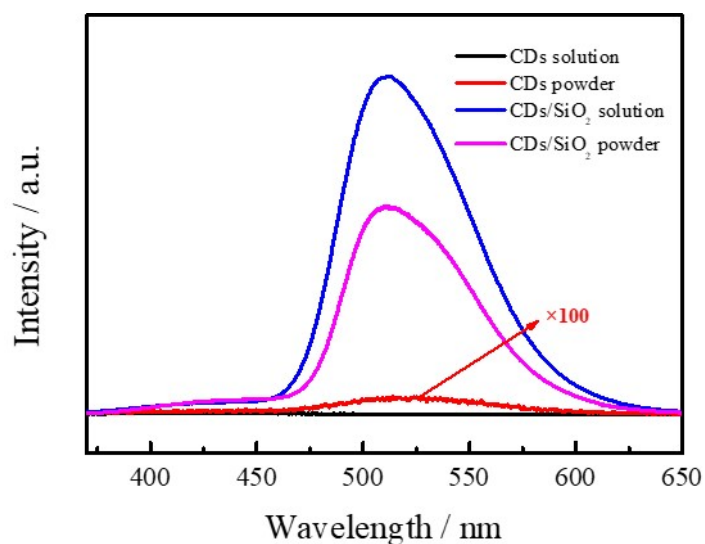


Figure S2. Afterglow spectra of solid-liquid CDs and solid-liquid CDs/SiO₂.

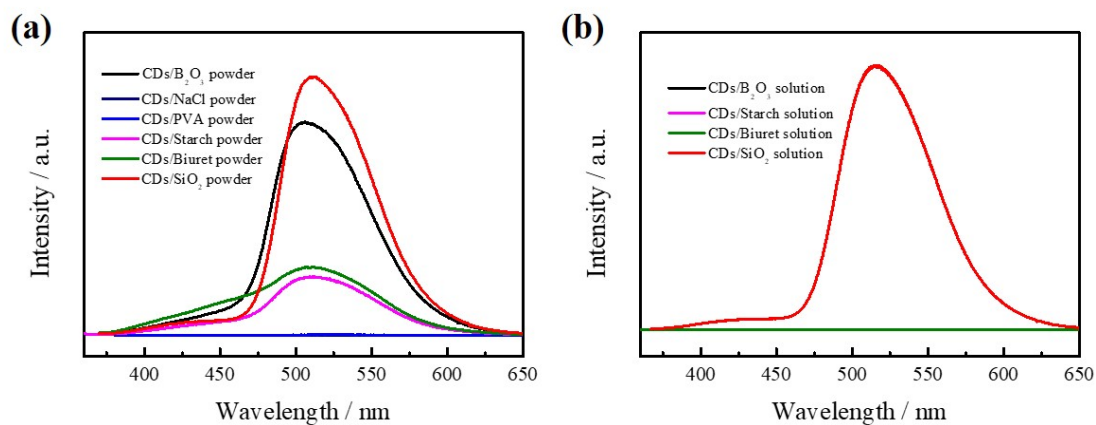


Figure S3 (a) Solid and (b) liquid afterglow spectra of CDs embedded in different matrices.

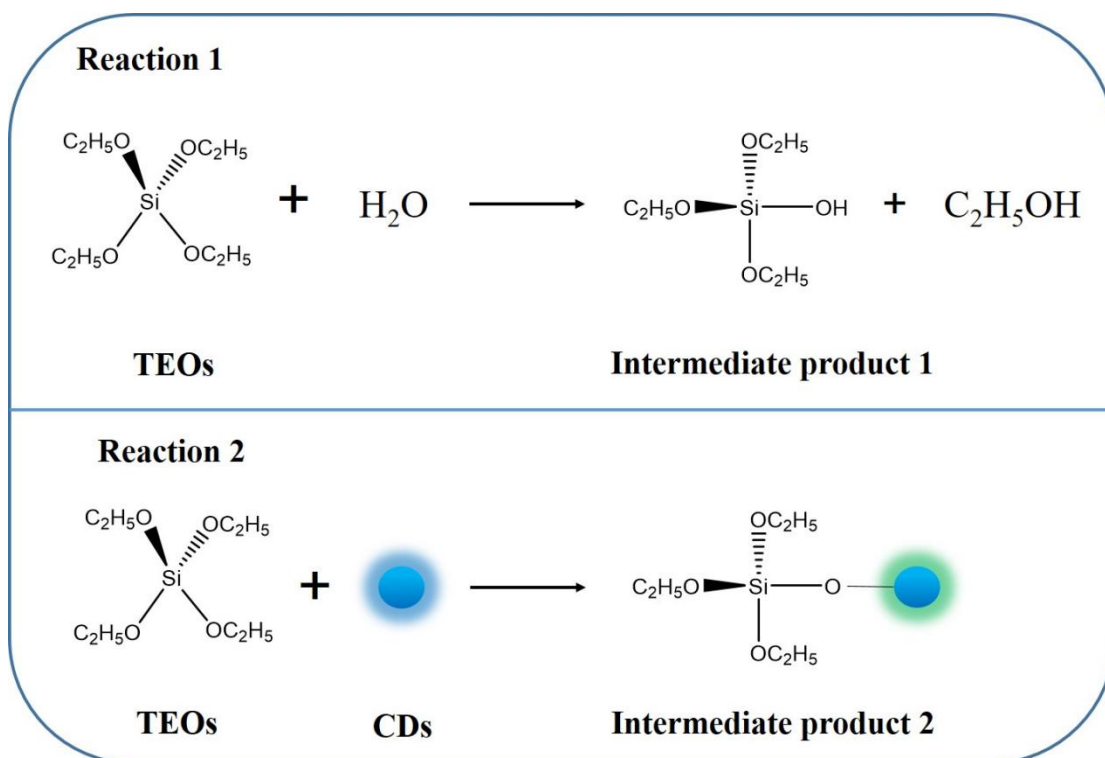


Figure S4. The mechanism of SiO₂ encapsulation of CDs.

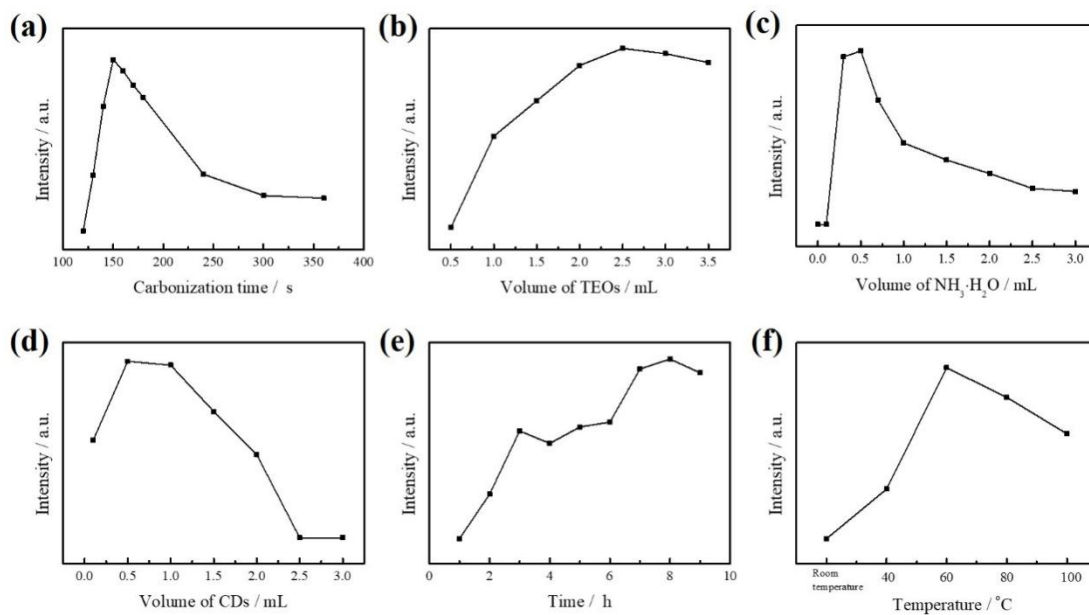


Figure S5. The phosphorescence intensity of CDs/SiO₂ solution with (a) different carbonization time, (b) different TEOs volumes, (c) different NH₃·H₂O volumes, (d) different CDs volumes, (e) different hydrolysis times, and (f) different hydrolysis temperature.

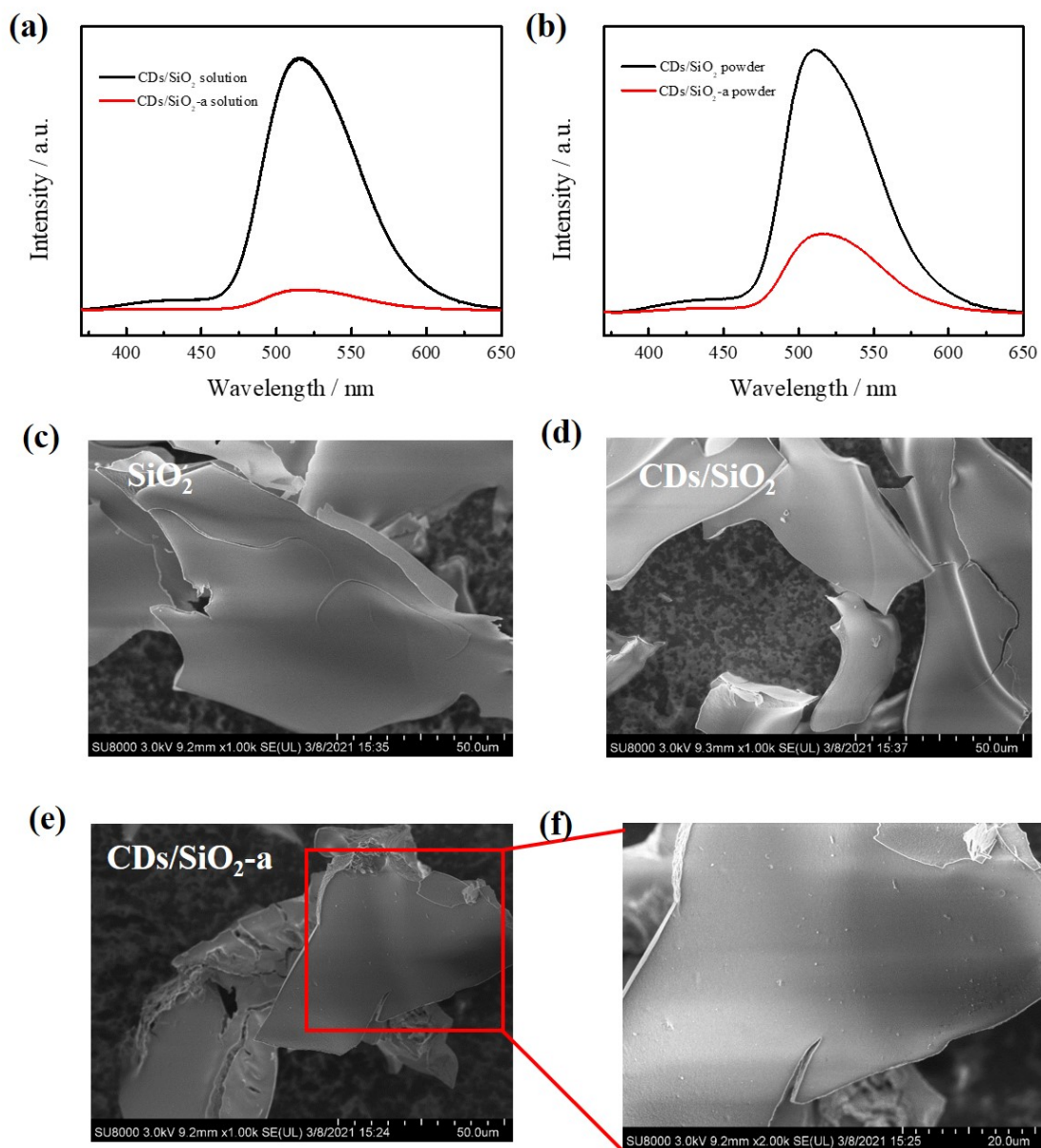


Figure S6. Afterglow spectra of CDs/SiO₂ and CDs/SiO₂-a (a) solutions and (b) powders. SEM images of (c) SiO₂, (d) CDs/SiO₂ and (e) CDs/SiO₂-a. (f) The enlarged images of corresponding areas

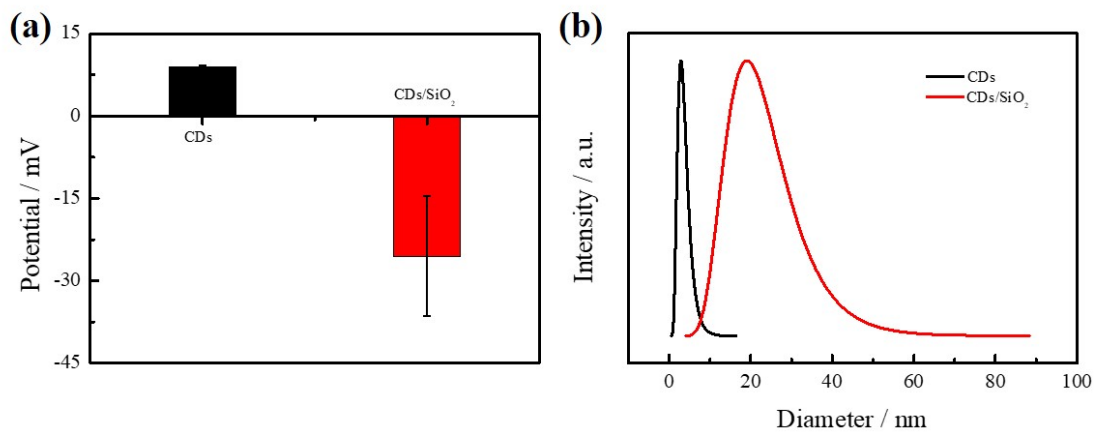


Figure S7. (a) Zeta potential and (b) hydrated particle size of CDs and CDs/SiO₂.

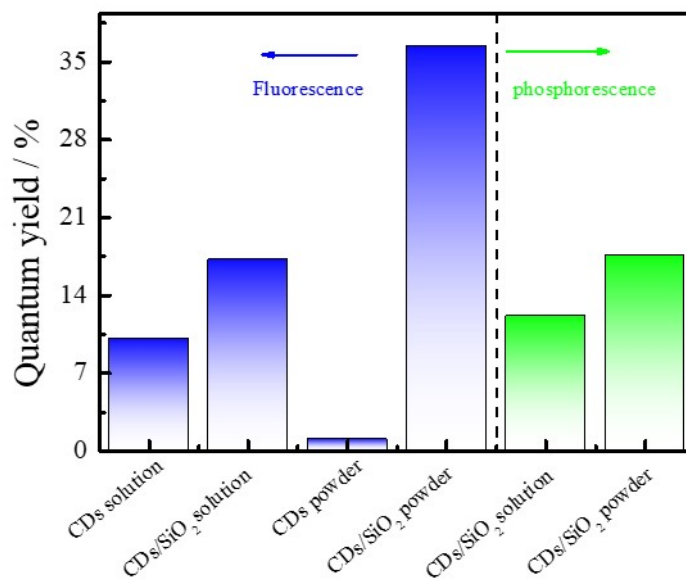


Figure S8. Fluorescence quantum yield of CDs solution, CDs/SiO₂ solution, CDs powder, CDs/SiO₂ powder and afterglow quantum yield of CDs/SiO₂ solution and CDs/SiO₂ powder.

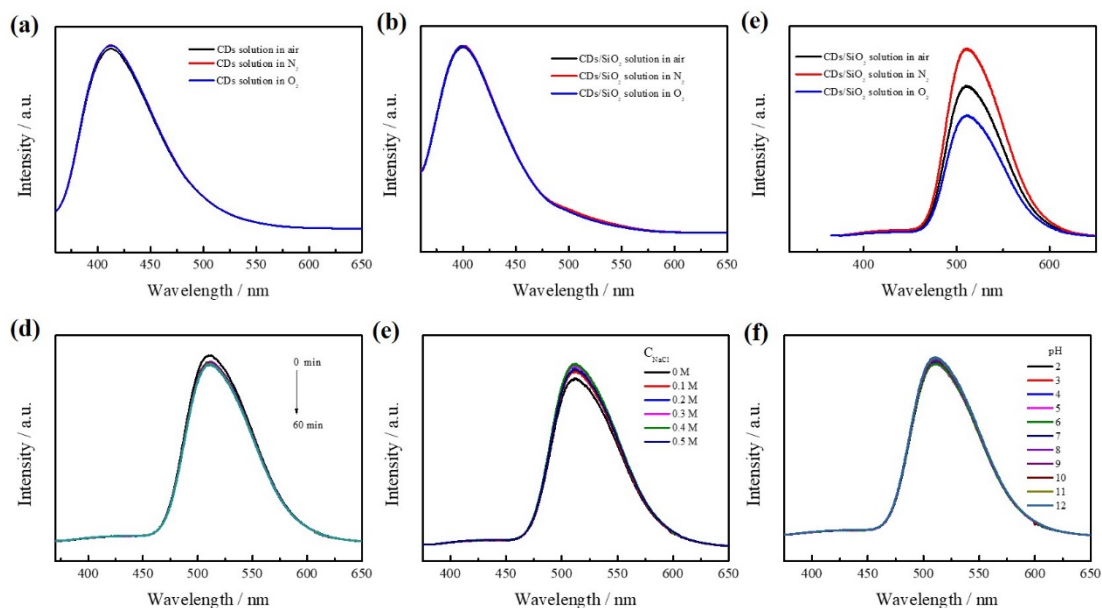


Figure S9. The fluorescence spectra of (a) CDs solution and (b) CDs/SiO₂ solution after purging with oxygen, nitrogen, or air for 60 min. The afterglow spectrum of CDs/SiO₂ solution (c) after purging with oxygen, nitrogen, or air for 60 min; The afterglow spectrum of CDs/SiO₂ solution under (d) different light time, (e) different pH and (f) different NaCl concentration

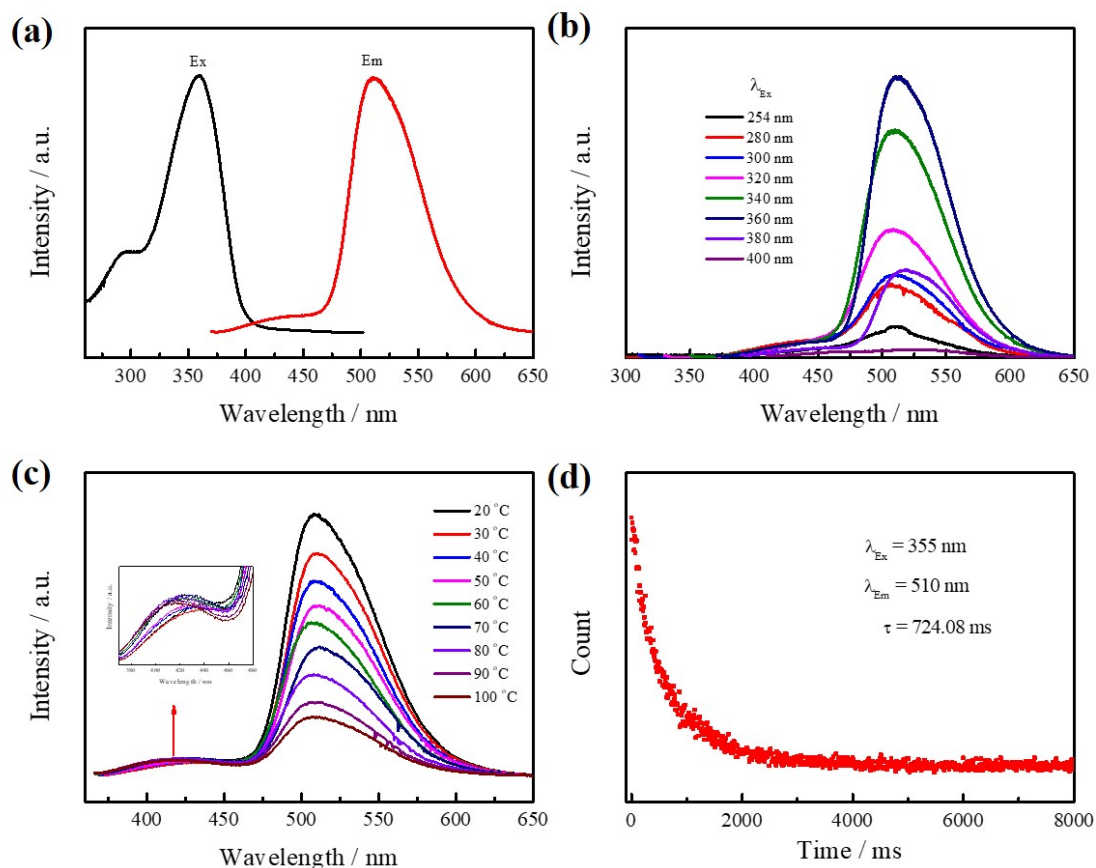


Figure S10. Afterglow excitation and emission spectra of CDs/SiO₂ powder. (b)

Afterglow emission spectra of CDs/SiO₂ powder at different excitation wavelengths; (c) Afterglow spectra of CDs/SiO₂ powder at different temperatures; (f) Afterglow decay curve of CDs/SiO₂ powder.

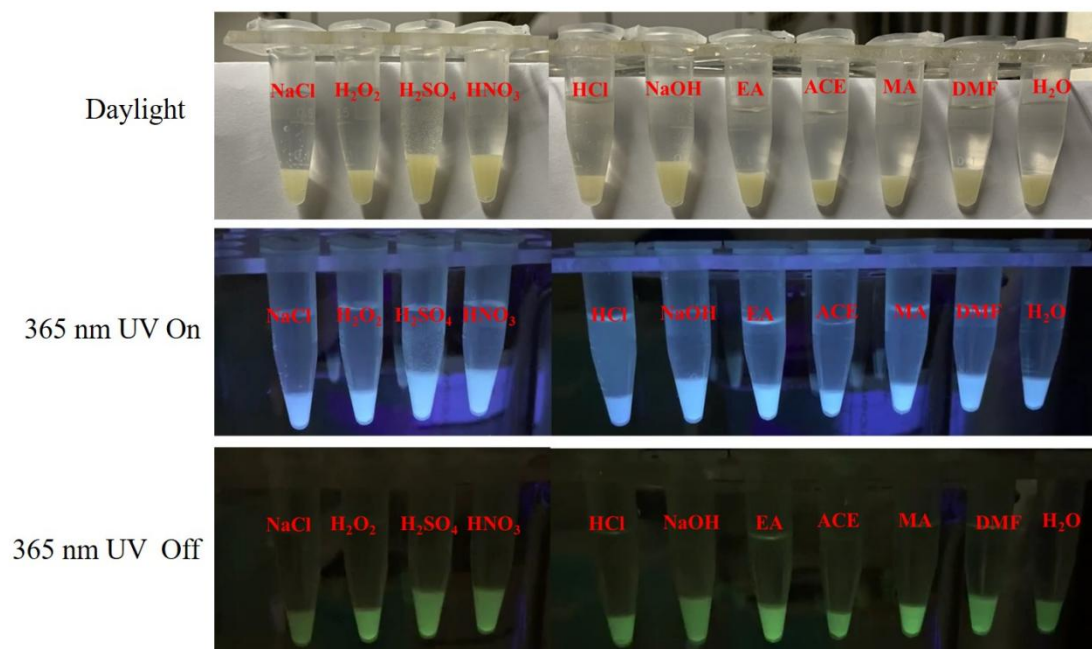


Figure S11. Digital photographs of CDs/SiO₂ powder in different solvents under daylight, excited with 365 nm UV lamp, and after switching off 365 nm UV lamp.

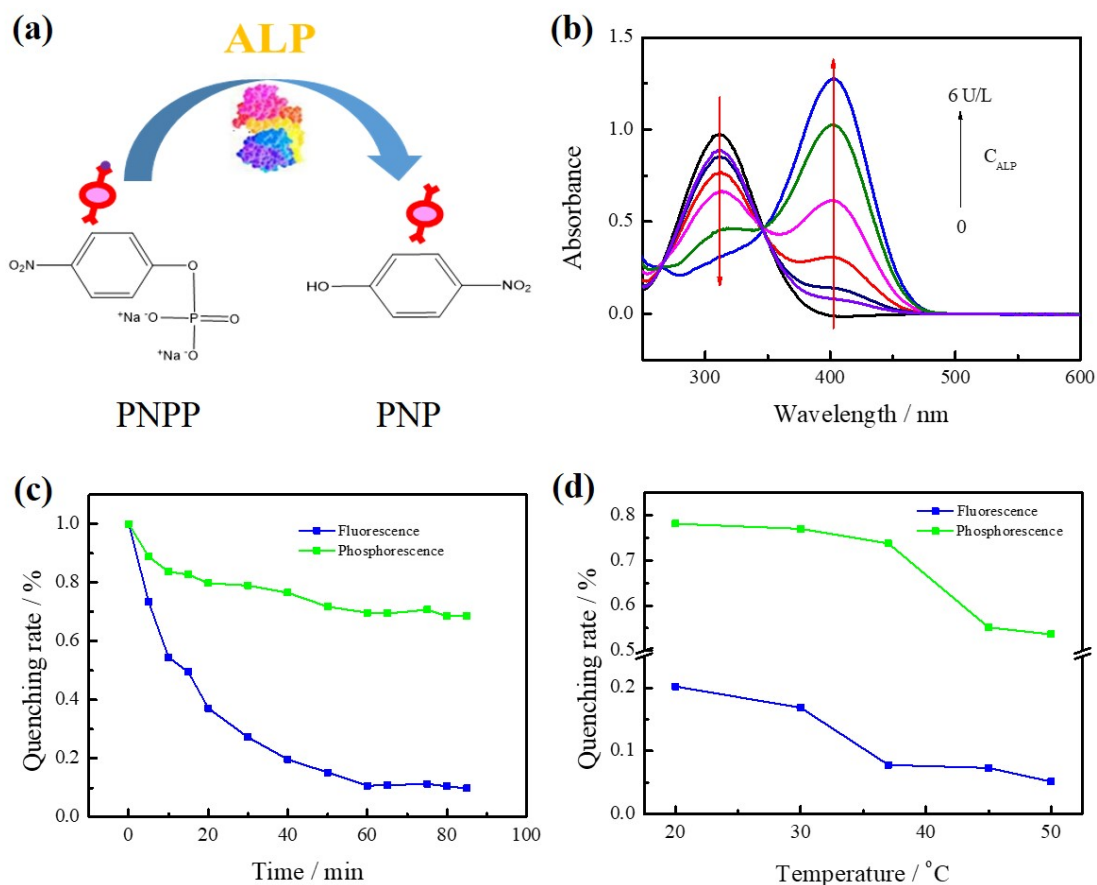


Figure S12. (a) Schematic diagram of ALP catalysis. (b) UV-visible absorption spectra of enzyme reaction solutions with different concentrations of ALP, 1 mM PNPP and 0.1 mM $MgSO_4$. The influence of (c) response time and (d) temperature on the detection of ALP.

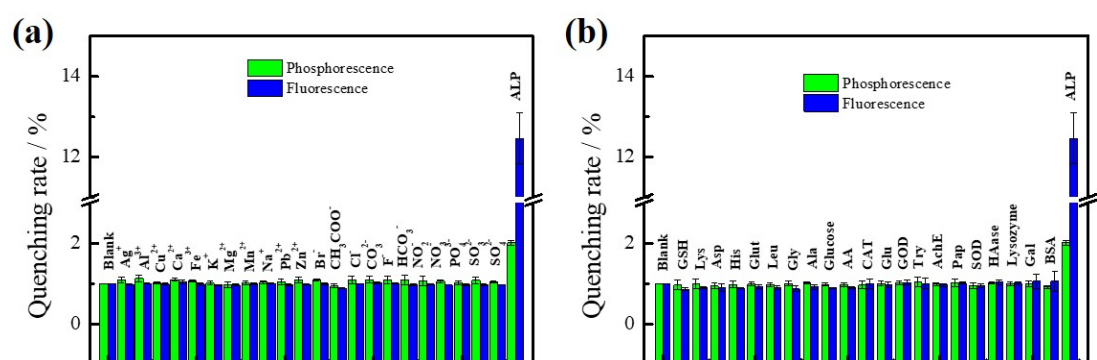
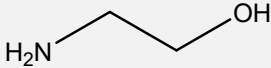
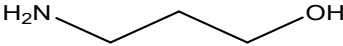
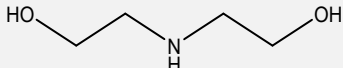
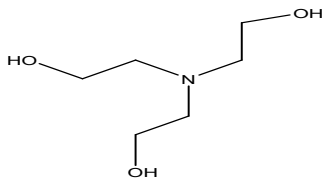
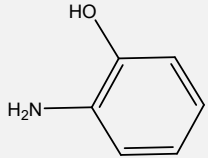
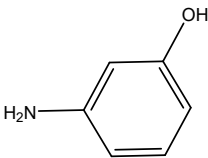
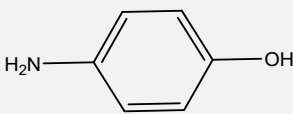
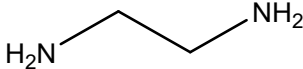
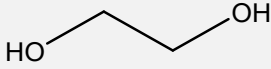


Figure S13. The effect of coexisting substances on CDs/ SiO_2 solution.

3. Table

Table S1 Summary of RTP properties of CDs/SiO₂ prepared by twelve kinds of CDs prepared by different precursors and synthetic methods

| Code name | Precursor 1 | Precursor 2 | Synthetic method | RTP |
|-----------|---|--------------------------------|------------------|--------|
| CDs |  | | | Strong |
| CDs-1 |  | | | Weak |
| CDs-2 |  | | | Weak |
| CDs-3 |  | | | Weak |
| CDs-4 |  | H ₃ PO ₄ | Microwave | None |
| CDs-5 |  | | | None |
| CDs-6 |  | | | None |
| CDs-7 |  | | | Medium |
| CDs-8 |  | | | None |

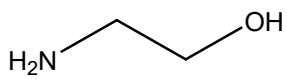
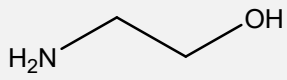
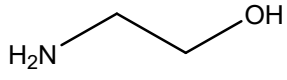
| | | | | |
|--------|---|--------------------------------|--------------|------|
| CDs-9 |  | H ₂ SO ₄ | | None |
| CDs-10 |  | H ₃ PO ₄ | Hydrothermal | None |
| CDs-11 |  | | Pyrolysis | None |

Table S2 Comparison of water-soluble CDs/SiO₂ with other reported water-soluble afterglow materials

| Long afterglow materials | Afterglow lifetime (ms) | Afterglow quantum yield (%) | Reference |
|--------------------------|-------------------------|-----------------------------|-----------|
| CDs-CA | 687 | - | [4] |
| Lu-DVDMS | 0.167 | 0.33 | [5] |
| PNDs | 0.5046 | 14.6 | [6] |
| CDs@SiO ₂ | 1640 | - | [7] |
| OSN1-T | 861 | 1.59 | [8] |
| C-C4-Br | 140 | 11 | [9] |
| m-PBCM | 710 | 10.2 | [10] |
| WSP-CND@silica | 1860 | 11.6 | [3] |
| CDs/SiO ₂ | 846.9 | 12.1 | This work |

Table S3 Comparison of this method and other methods for detecting ALP

| Sensor | Linear range (U/L) | LOD (U/L) | Reference |
|-----------------------------------|--------------------------|-----------------------|-----------|
| MoS ₂ QDs | 0-5 | 0.1 | [11] |
| g-C ₃ N ₄ | 0.1-1000 | 0.08 | [12] |
| CDs | 2.5-40 | 1 | [13] |
| CDs-AuNCs ₃ | 0.12-15 | 0.05 | [14] |
| N-CDs | 0.05-40 | 0.02 | [15] |
| CDs-V ₂ O ₅ | 0.1-30 | 0.04 | [16] |
| N-GQDs | 0.1-5 | 0.07 | [17] |
| CDs | 5-200 | 0.8 | [18] |
| CDs-MnO ₂ | 0.1-500 | 0.02 | [19] |
| CDs/SiO ₂ | 0.025-1.25(Fluorescence) | 0.00875(Fluorescence) | This work |
| | 0.5-50(Phosphorescence) | 0.186(Phosphorescenc) | |

Reference

- [1] L. Wang, S.J. Zhu, H.Y. Wang, Y.F. Wang, Y.W. Hao, J.H. Zhang, Q.D. Chen, Y.L. Zhang, W. Han, B. Yang, H.B. Sun, Unraveling Bright Molecule-Like State and Dark Intrinsic State in Green-Fluorescence Graphene Quantum Dots via Ultrafast Spectroscopy, *Advanced Optical Materials* 1(3) (2013) 264-271.
- [2] W. Sun, Y.X. Du, Y.Q. Wang, Study on fluorescence properties of carbogenic nanoparticles and their application for the determination of ferrous succinate, *Journal of Luminescence* 130(8) (2010) 1463-1469.
- [3] Y.-C. Liang, S.-S. Gou, K.-K. Liu, W.-J. Wu, C.-Z. Guo, S.-Y. Lu, J.-H. Zang, X.-Y. Wu, Q. Lou, L. Dong, Y.-F. Gao, C.-X. Shan, Ultralong and efficient phosphorescence from silica confined carbon nanodots in aqueous solution, *Nano Today* 34 (2020) 100900.
- [4] Q. Li, M. Zhou, M. Yang, Q. Yang, Z. Zhang, J. Shi, Induction of long-lived room temperature phosphorescence of carbon dots by water in hydrogen-bonded matrices, *Nat Commun* 9(1) (2018) 734.
- [5] L.X. Zang, H.M. Zhao, Lutetium-containing sinoporphyrin sodium: a water-soluble photosensitizer with balanced fluorescence and phosphorescence for ratiometric oxygen sensing, *Rsc Adv* 10(54) (2020) 32938-32945.
- [6] H.F. Shi, L. Zou, K.W. Huang, H. Wang, C. Sun, S. Wang, H.L. Ma, Y.R. He, J.P. Wang, H.D. Yu, W. Yao, Z.F. An, Q. Zhao, W. Huang, A Highly Efficient Red Metal-free Organic Phosphor for Time-Resolved Luminescence Imaging and Photodynamic Therapy, *Acs Appl Mater Inter* 11(20) (2019) 18103-18110.
- [7] W. Li, S. Wu, X. Xu, J. Zhuang, H. Zhang, X. Zhang, C. Hu, B. Lei, C.F. Kaminski, Y. Liu, Carbon Dot-Silica Nanoparticle Composites for Ultralong Lifetime Phosphorescence Imaging in Tissue and Cells at Room Temperature, *Chem Mater* 31(23) (2019) 9887-9894.
- [8] X. Zhen, Y. Tao, Z.F. An, P. Chen, C.J. Xu, R.F. Chen, W. Huang, K.Y. Pu, Ultralong Phosphorescence of Water-Soluble Organic Nanoparticles for In Vivo Afterglow Imaging, *Adv Mater* 29(33) (2017) 1606665.
- [9] S.M.A. Fatemina, Z. Mao, S.D. Xu, Z.Y. Yang, Z.G. Chi, B. Liu, Organic Nanocrystals with Bright Red Persistent Room-Temperature Phosphorescence for Biological Applications, *Angew Chem Int Edit* 56(40) (2017) 12160-12164.
- [10] Z. He, H. Gao, S. Zhang, S. Zheng, Y. Wang, Z. Zhao, D. Ding, B. Yang, Y. Zhang, W.Z. Yuan, Achieving Persistent, Efficient, and Robust Room-Temperature Phosphorescence from Pure Organics for Versatile Applications, *Adv Mater* 31(18) (2019) e1807222.
- [11] Y. Zhong, F. Xue, P. Wei, R. Li, C. Cao, T. Yi, Water-soluble MoS₂ quantum dots for facile and sensitive fluorescence sensing of alkaline phosphatase activity in serum and live cells based on the inner filter effect, *Nanoscale* 10(45) (2018) 21298-21306.
- [12] M.H. Xiang, J.W. Liu, N. Li, H. Tang, R.Q. Yu, J.H. Jiang, A fluorescent graphitic carbon nitride nanosheet biosensor for highly sensitive, label-free detection of alkaline phosphatase, *Nanoscale* 8(8) (2016) 4727-4732.

- [13] W.J. Kang, Y.Y. Ding, H. Zhou, Q.Y. Liao, X. Yang, Y.G. Yang, J.S. Jiang, M.H. Yang, Monitoring the activity and inhibition of alkaline phosphatase via quenching and restoration of the fluorescence of carbon dots, *Microchimica Acta* 182(5-6) (2015) 1161-1167.
- [14] H.J. Liu, L. Jia, Y.X. Wang, M.Y. Wang, Z.D. Gao, X.Q. Ren, Ratiometric fluorescent sensor for visual determination of copper ions and alkaline phosphatase based on carbon quantum dots and gold nanoclusters, *Anal Bioanal Chem* 411(12) (2019) 2531-2543.
- [15] Y. Zhang, Y. Nie, R. Zhu, D. Han, H. Zhao, Z. Li, Nitrogen doped carbon dots for turn-off fluorescent detection of alkaline phosphatase activity based on inner filter effect, *Talanta* 204 (2019) 74-81.
- [16] R.F. Zhu, W.Y. Huang, X.F. Ma, Y.H. Zhang, C.C. Yue, W.H. Fang, Y. Hu, J. Wang, J.Q. Dang, H. Zhao, Z.X. Li, Nitrogen-doped carbon dots-V₂O₅ nanobelts sensing platform for sensitive detection of ascorbic acid and alkaline phosphatase activity, *Analytica Chimica Acta* 1089 (2019) 131-143.
- [17] J.J. Liu, D.S. Tang, Z.T. Chen, X.M. Yan, Z. Zhong, L.T. Kang, J.N. Yao, Chemical redox modulated fluorescence of nitrogen-doped graphene quantum dots for probing the activity of alkaline phosphatase, *Biosensors & Bioelectronics* 94 (2017) 271-277.
- [18] P. Song, Q. Liu, Y. Zhang, W. Liu, M. Meng, Y.M. Yin, R.M. Xi, The chemical redox modulated switch-on fluorescence of carbon dots for probing alkaline phosphatase and its application in an immunoassay, *Rsc Adv* 8(1) (2018) 162-169.
- [19] K. Shao, Y. Yang, S. Ye, D. Gu, T. Wang, Y. Teng, Z. Shen, Z. Pan, Dual-colored carbon dots-based ratiometric fluorescent sensor for high-precision detection of alkaline phosphatase activity, *Talanta* 208 (2020) 120460.